



Journal of Advanced Research in Fluid Mechanics and Thermal Sciences

Journal homepage:
https://semarakilmu.com.my/journals/index.php/fluid_mechanics_thermal_sciences/index
ISSN: 2289-7879



Comparison of Thermal Effectiveness and Crevice Corrosion Risk of Fin Geometry on All-Aluminum Microchannel Heat Exchangers

Hossain Ahmed^{1,*}, Seifollah Nasrazadani¹, Hamid Sadat¹

¹ Department of Mechanical Engineering, University of North Texas, Denton, Texas 76207, United States

ARTICLE INFO

Article history:

Received 6 January 2023
Received in revised form 11 April 2023
Accepted 18 April 2023
Available online 8 May 2023

Keywords:

Computational Fluid Dynamic (CFD);
Microchannel Heat Exchanger (MCHE);
crevice corrosion; pitting corrosion;
corrosion hotspot

ABSTRACT

All-aluminum microchannel heat exchangers have recently gained popularity in the heating, ventilation, and air conditioning industry. Despite their attractive thermal performance design, these heat exchangers make coils used in automotive, commercial, and residential applications prone to crevice corrosion. This study uses high-fidelity conjugate heat transfer simulations to model a micro channel heat exchanger system that includes fins and tubes with crossflow to compare their thermal effectiveness to gain insight into potential crevice corrosion of the MCHE alloy. This study considers three fin geometries (louver, step, and saw) with the same tube and circular shape microchannel and identifies the corrosion hot spot and thermal effectiveness. A predicted flow field also identifies crevices between fins and tube surfaces as critical corrosion hot spots often associated with low-velocity regions. The crevice volumes for the louver, step, and saw fin shapes are calculated as $2.719 \times 10^{-5} \text{ in}^3$, $3.297 \times 10^{-5} \text{ in}^3$ and $3.508 \times 10^{-4} \text{ in}^3$ respectively. Results also show that the same circular microchannel louver shape fin has higher effectiveness than the step and saw shape fin. The thermal effectiveness for microchannel tubes with louver, step, and saw shape fins are 0.337, 0.20737, and 0.2895, respectively.

1. Introduction

The utilization of all-aluminium microchannel heat exchangers (MCHEs) in HVAC systems and automobiles has gained popularity due to their low cost, lightweight nature, and enhanced thermal efficiency compared to copper round tube and plate-fin (RTPF) heat exchangers. The use of all-aluminium alloys in heat exchanger construction is also advantageous in terms of corrosion resistance, effectively addressing the issue of galvanic corrosion present in conventional RTPF heat exchangers. However, despite the passive nature of aluminium alloys and the use of all-aluminium materials to mitigate galvanic corrosion, instances of corrosion in MCHE systems have been reported [1-8]. The majority of heat exchanger failures occur due to harsh operating environments. Crevice corrosion, resulting from salt deposition and fouling, has been observed [1]. Yoshino *et al.*, [9] highlighted intergranular corrosion (IGC) caused by contact between the fin and the microstructure,

* Corresponding author.

E-mail address: hossainahmed@my.unt.edu

<https://doi.org/10.37934/arfmts.105.2.192203>

as well as variations in chemical composition. Areas susceptible to crevice corrosion tend to accumulate deposits and retain moisture for extended periods, leading to increased corrosion. The region between the fin and tube is particularly vulnerable to crevice corrosion due to limited fluid flow or very low fluid velocities. Stagnant regions harbour corrosive salts and other contaminants, resulting in the formation of pits of varying sizes that eventually lead to tube perforation. Faes *et al.*, [8] have also observed localized corrosion in heat exchangers. Although aluminium alloys form a protective film, they are still prone to pitting [10]. Pitting begins with surface damage to the protective layers, and over time, these pits enlarge and penetrate the heat exchanger tubes. Corrosion products present in the atmosphere initiate this pitting process, with factors such as chloride content, high temperatures, and low pH values promoting pitting corrosion. Localized damage to the metal protective film during the construction phase of MCHEs can also initiate pitting [11]. Crevice corrosion, a localized form of corrosion, occurs due to a different local environment compared to the bulk environment. Oxygen depletion, for example, can occur in crevices or shielded areas where stagnant conditions prevail. This oxygen concentration disparity influences the occurrence of crevice corrosion. Additionally, enlarging the cathode area can increase the corrosion rate while potentially reducing the crevice area [12]. In plate heat exchangers, crevices are typically found at the joining points of metals [8]. Ranjbar *et al.*, [13] conducted experimental investigations on flow-induced corrosion and identified corrosion occurrences in regions with low fluid velocities.

Unlike the importance of corrosion in MCHEs, the studies have been mostly conducted on the transport phenomena within microchannels or the influence of fin and microchannel geometry on heat exchanger performance [14-22]. Researchers also improved heat exchanger performance using nanofluid with different nanoparticle shapes [23,24]. Hasan *et al.*, [22] numerically investigated the hydrodynamics and thermal behaviors of different microchannel geometries and identified the best ones. He found that the effectiveness increases when the Re decreases due to increased flow velocity. For example, for square shape microchannel, the effectiveness increases from 0.15 to 0.5 for the Re number change from 900 to 50. The limitation of the previous studies is that none of those considered environmental airflow's effect. Therefore, the influence of environmental airflow and the corrosion aspects associated with local flow patterns has been always overlooked. In this study, the thermal performance and corrosion of a MCHC with three different fin geometries (louver, step, and saw) combined with a circular microchannel is numerically investigated. To the best of our knowledge, this investigation is the first to assess the crevice corrosion risk associated with different fin geometries in MCHCs using CFD (Computational Fluid Dynamic) simulation.

2. Methodology

2.1 Geometry

This CFD analysis focuses on a circular microchannel with three distinct fin shapes. To optimize computational efficiency, the CFD model is constructed using a small section of an MCHC tube with attached fins of a five-step shape, as depicted in Figure 1. Considering the symmetric conditions of the MCHC and to reduce computational costs, only half of the fins' height on each side of the tube is taken into account. The dimensions of the analysed MCHC section are $(0.4 \times 0.07 \times 0.05)$ (length \times width \times height) cubic inches. Three different fin geometries, namely step, louver, and saw shapes, are investigated for the tube. While all geometries feature the same circular microchannel and solid tube, their fin designs vary. In the simulations, a coordinate system is defined, with the Z-axis aligned with the microchannel axis, the Y-axis parallel to the fin surfaces and tube height, and the X-axis corresponding to the tube width. Table 1 provides specific dimension details for the microchannel.

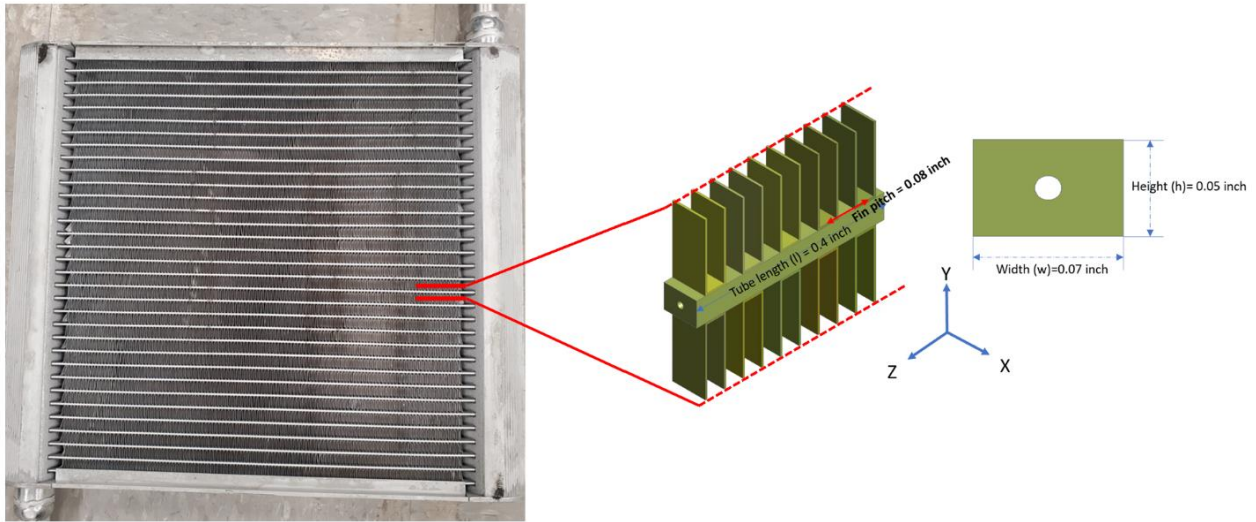


Fig. 1. Schematic diagram of a characteristic part of MCHX

Table 1

Geometry specification of MCHE

Microchannel Shape	Circular
Parameter	Value
Tube length l (inch)	0.4
Tube height h (inch)	0.05
Tube Width w (inch)	0.07
Hydraulic Diameter (inch)	0.0125
Microchannel volume (inch ³)	4.8819×10^{-5}
Fin type	Step/Louver/Saw
Fin thickness (inch)	0.0003937
Fin height (inch)	0.14295
Fin pitch (inch)	0.08

2.2 CFD Method

The ANSYS Fluent software was employed to simulate the segmental MCHE (Microchannel Heat Exchanger). Below governing equations for mass, momentum, and energy for steady-state, incompressible flow are solved

$$\nabla \cdot \vec{v} = 0 \quad (1)$$

$$\rho \frac{\partial}{\partial t} (\vec{v}) + \nabla \cdot (\rho \vec{v} \vec{v}) = -\nabla p + \mu \nabla^2 \vec{v} + F \quad (2)$$

$$\rho C_p \frac{\partial T}{\partial t} + \rho C_p \vec{v} \cdot \nabla T = \nabla \cdot (k \nabla T) + \phi \quad (3)$$

In these equations, p represents the static pressure, μ denotes molecular viscosity, \vec{v} represents the velocity field, T signifies temperature, C_p represents the specific heat at constant pressure, F represents the body force, and ϕ represents the dissipation function, which accounts for the work done against viscous forces.

For the solid side, the energy governing equation takes the following form

$$\rho C_p \frac{\partial T}{\partial t} = \nabla \cdot (k \nabla T) + \Phi \quad (4)$$

The finite volume method was employed to discretize the governing equations and boundary conditions. The fluids were assumed to be incompressible, and the flow was considered to be laminar and in a steady state. The influence of gravity was neglected in this simulation. The Couple algorithm was used for pressure-velocity coupling to ensure mass conservation and obtain a pressure field. The convection-diffusion terms were discretized using the second-order Upwind scheme. The grid parameters utilized in this study are provided in Table 2.

Table 2

Grid sizes	
Domain	Grid
Inlet Air-Domain	1437862
Air Between Fins	1516795
Outlet Air-Domain	1508529
Microchannel	43992
Fin	815462 (Step)
Rectangular Tube	3339600
All Domains	8662240

2.3 Boundary Conditions

The computational domain consists of three main regions: the crossflow (air) domain, the microchannel flow domain, and the solid region. Figure 2 provides a schematic view of the computational domain. The crossflow domain is divided into the inlet region, the region between fins, and the outlet region. It extends from $X=0.5$ inch to $X=1.25$ inch, with the width and height matching that of the simulated section of the MCHE. The microchannel flow domain has a length of $l=0.4$ inch and a cylindrical geometry with a diameter of 0.0125 inch.

Table 3 outlines the boundary conditions utilized in this study. Furthermore, Figure 3 illustrates the triangular prism and hexahedral mesh generated for the circular MCHE with step fins.

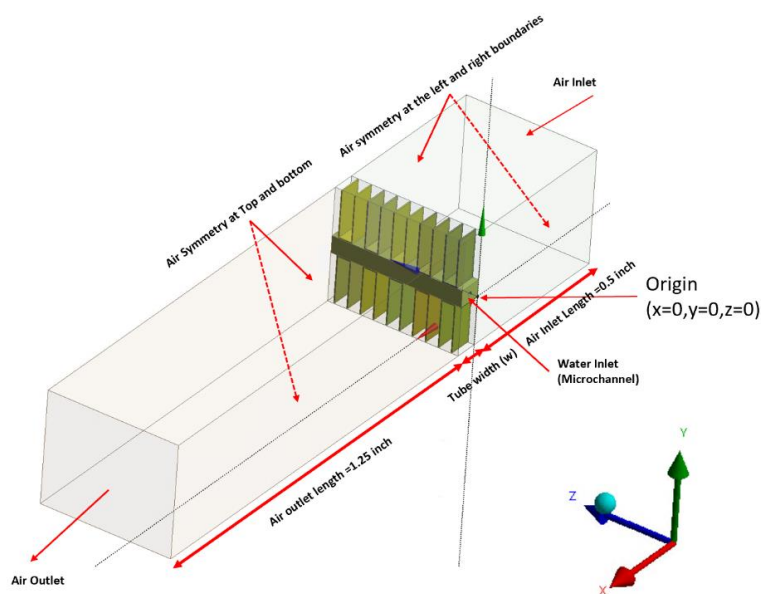


Fig. 2. Computational domain for MCHE with Step shape fin

Table 3

Boundary conditions of the computational domains

Domains	Parts	Boundary conditions
Microchannel	Inlet (water inlet, z-direction)	Velocity inlet; $U_w = 0.2 \frac{m}{s}$, Inlet temperature of the water, $T_{w,in} = 50^\circ C$
	Outlet	Pressure outlet
	Wall	Via system coupling with solid for temperature; No-slip boundary condition for velocity
Solid (aluminum)	Inlet	Inlet temperature, $T_s = 40^\circ C$
	Outlet	Heat flux=0
	Wall	Via system coupling with air for temperature; No-slip boundary condition for velocity
Fin (aluminum)	Top fin and bottom fin boundaries	Symmetric
Crossflow	Inlet (air inlet, x-direction)	Velocity inlet; $U_a = 16 \frac{m}{s}$ (Inlet temperature of the air, $T_a = 26.85^\circ C$
	Outlet	Pressure outlet
	Side boundaries	Symmetric

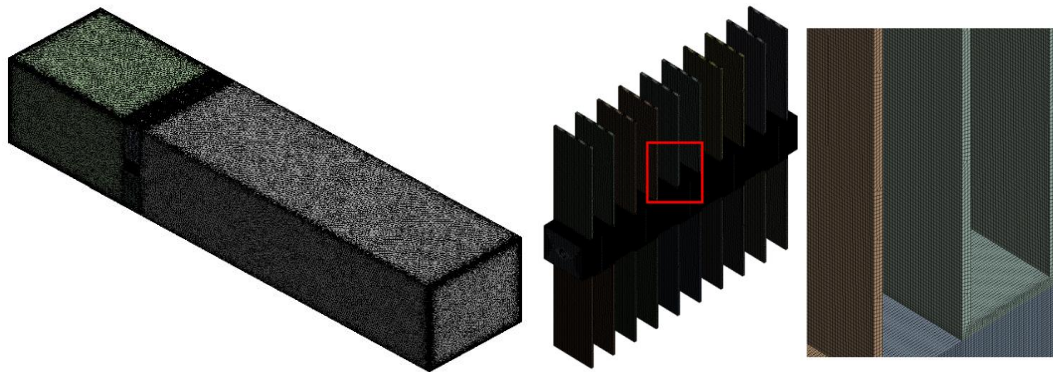


Fig. 3. Details of triangular prism and hexahedral mesh of circular MCHC with step fin

2.4 Grid Verification and Validation Study

Grid verification was performed solely for the microchannel flow, utilizing coarse, medium, and fine mesh sizes with 40 thousand, 90 thousand, and 160 thousand grids, respectively. The analysis of the results indicated that the predicted centerline velocity exhibited a change of 1.02% from coarse to medium grid and 0.36% from medium to fine grid, suggesting that the results were reasonably insensitive to the grid size. To further validate the results, Figure 4 illustrates a comparison between the predicted velocity profile and the theoretical or analytical profile. Once again, the results demonstrate good agreement between the predicted and theoretical profiles. Consequently, the coarse grid size was employed for all simulations.

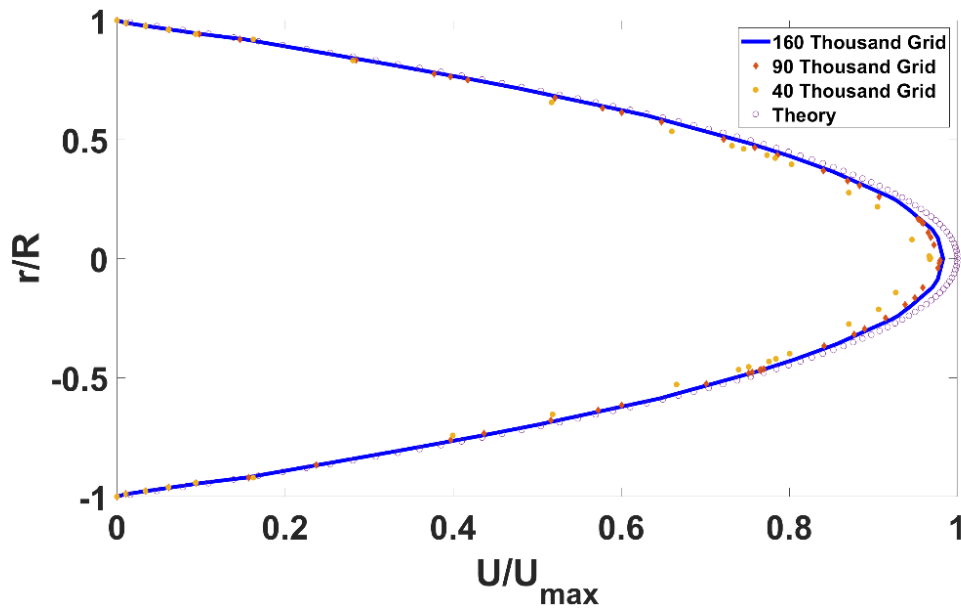


Fig. 4. Verification analysis of microchannel flow

2.5 Variables of Interest

This study focused on examining field variables, namely velocity, pressure, and temperature, to analyze the performance of the heat exchanger. The thermal effectiveness of the heat exchanger, which quantifies the actual heat transfer relative to the maximum possible heat transfer, was assessed using

$$\epsilon_{\text{circular channel}} = \frac{q}{q_{\text{max}}} = \frac{C_h(T_{w,\text{in}} - T_{w,\text{out}})}{C_{\text{min}}(T_{w,\text{in}} - T_{a,\text{in}})} \quad (5)$$

Additionally, the study investigated corrosion hot spots by analysing the velocity field.

3. Results

The velocity contour of the entire computational domain is depicted in Figure 5. Flow separation is observed at the contact point between the crossflow (airflow) and the solid tube, causing the solid tube to be immersed within the separated flow region. The crossflow velocity outside the separated region gradually increases, due to the increase of the wake thickness until $X=0.91$ inch. Subsequently, the crossflow velocity starts to decrease.

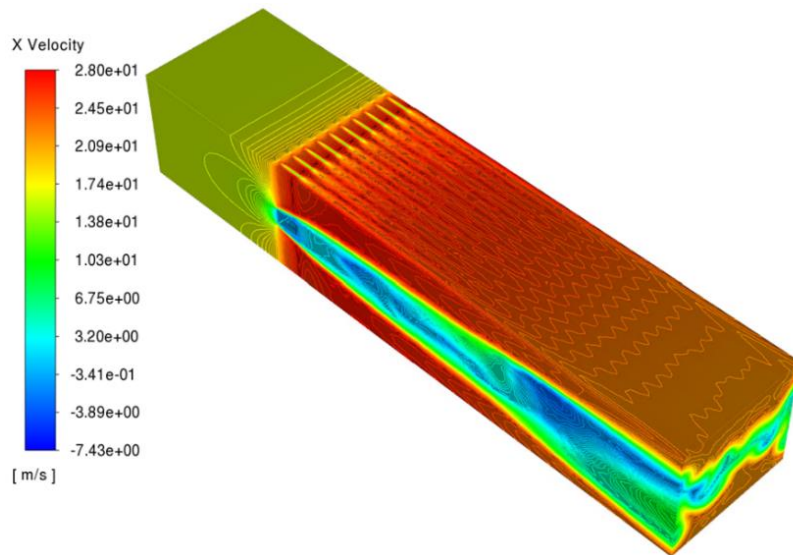


Fig. 5. Velocity contour of the whole computational domain

Figure 6 to Figure 8 provide the velocity contour surrounding the circular MCHE. At $X=0.035$ inch (origin as described in Figure 2), the boundary layer formed near the solid side tube exhibits zero or low velocity. The thickness of this boundary layer varies along the fin pitch, resulting in a larger boundary layer thickness in region A, enclosed by each fin, compared to region B, located in the gap between two consecutive fins. As the crossflow moves away from the tube and fin, the velocity increases between the fins, reaching up to ~ 28 m/s. This velocity is approximately 70% higher than the inlet velocity. These low-velocity regions, A and B, serve as hotspots for pitting and crevice corrosion. Pitting corrosion and crevice corrosion are both localized forms of corrosion that result in rapid penetration at small specific areas. The occurrence of these corrosion types can be effectively controlled by ensuring adequate flow velocities to prevent stagnation or the accumulation of solid materials. Pitting corrosion is more likely to occur during periods of shutdown when there is no flow, creating an environment conducive to the formation of concentration cells. The corrosion hot spot area can be determined by determining the volume of the low velocity region (blue region) per fin pitch. Our result shows that saw shaped fin has more hot spot volume on top surface of the solid which is $3.508 \times 10^{-3} \text{inch}^3$. The hot spot volume for the louver and step shape fin are $2.719 \times 10^{-5} \text{inch}^3$ and $3.297 \times 10^{-5} \text{inch}^3$.

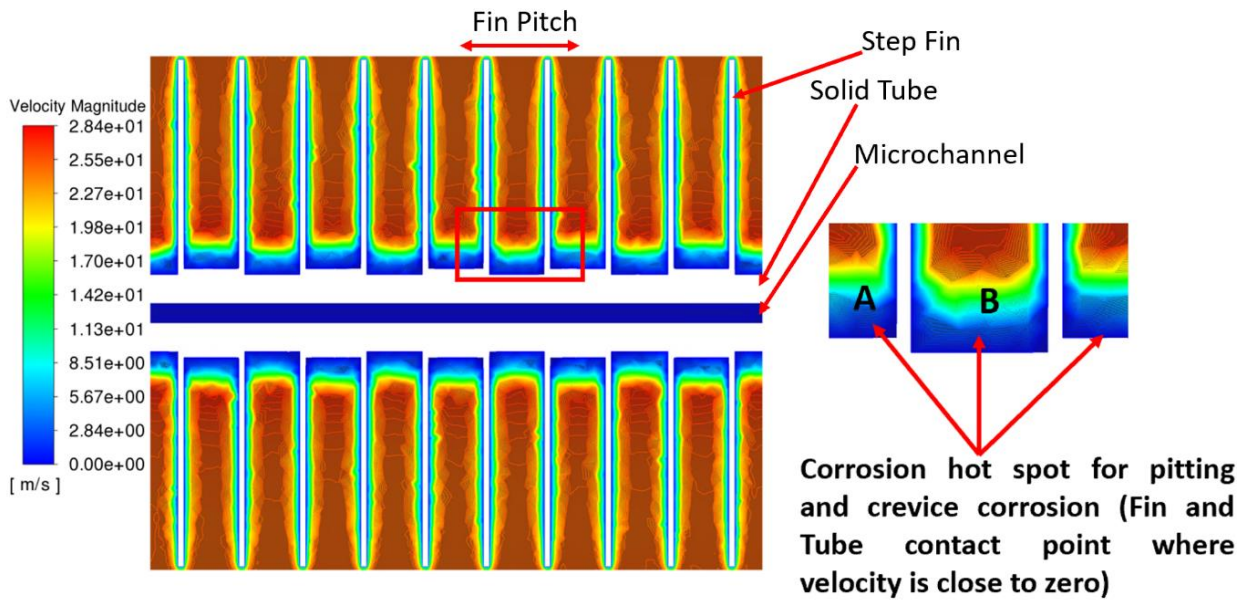


Fig. 6. Stagnation region identification for step-shaped fin geometry at X=0.035 inch

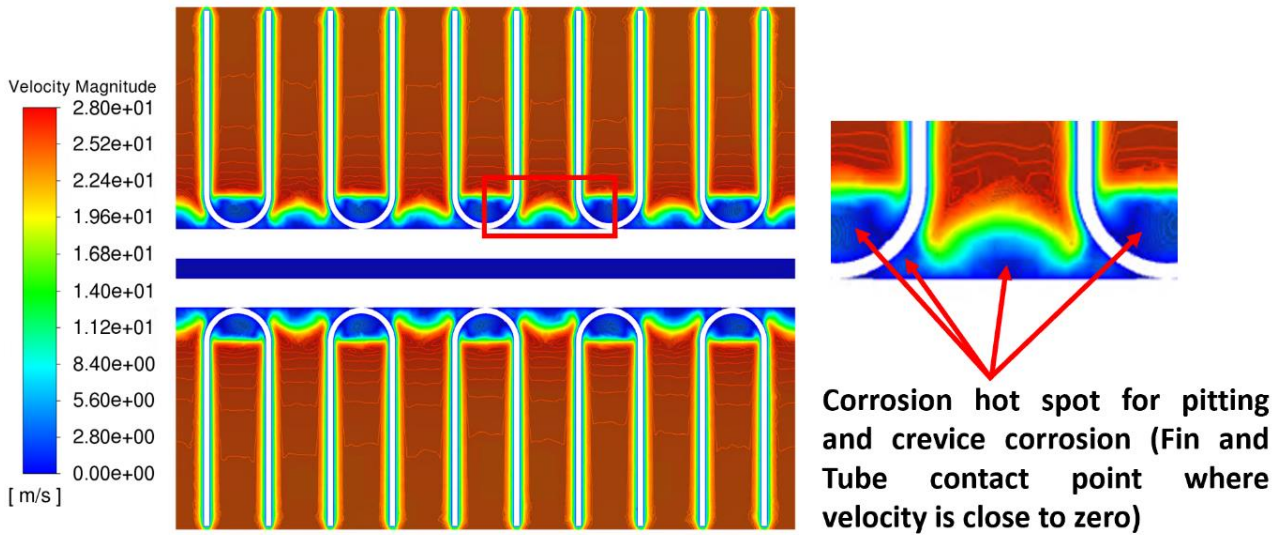


Fig. 7. Stagnation region identification for louver shaped fin geometry at X=0.035 inch

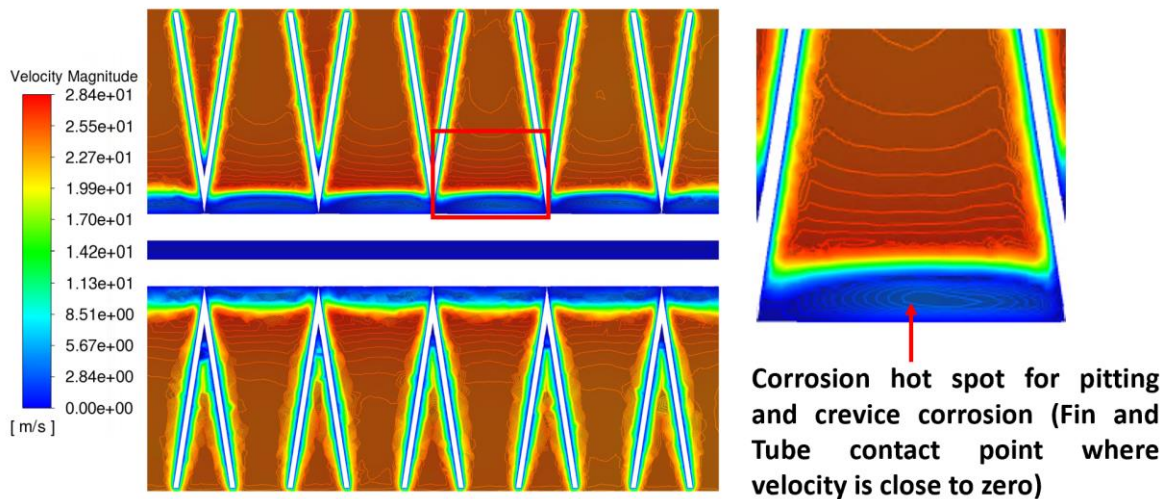


Fig. 8. Stagnation region identification for Saw shaped fin geometry at X=0.035 inch

Figure 9 provides experimental evidence conducted in our laboratory, illustrating the occurrence of pitting corrosion in the vicinity of the fin and solid surface. Additionally, the experimental work confirms that crevice corrosion takes place at the junction between the fin and solid surfaces.

Scanning electron microscopy (SEM) was employed to assess the damaged regions in the corroded MCHE samples. After being exposed to a corrosive atmosphere within the corrosion chamber for a period exceeding 104 days, the MCHE samples were collected [25]. Figure 9 displays a corroded crevice area located near the junction of the fin and solid surfaces. This condition differs from other forms of failure, such as vibration failure, where the metal is abruptly fractured without the presence of pits. Crevice corrosion tends to occur under conditions of relatively low or zero velocity. Controlling the velocity to ensure sufficient flow is crucial in preventing stagnation and restraining the occurrence of such corrosion.

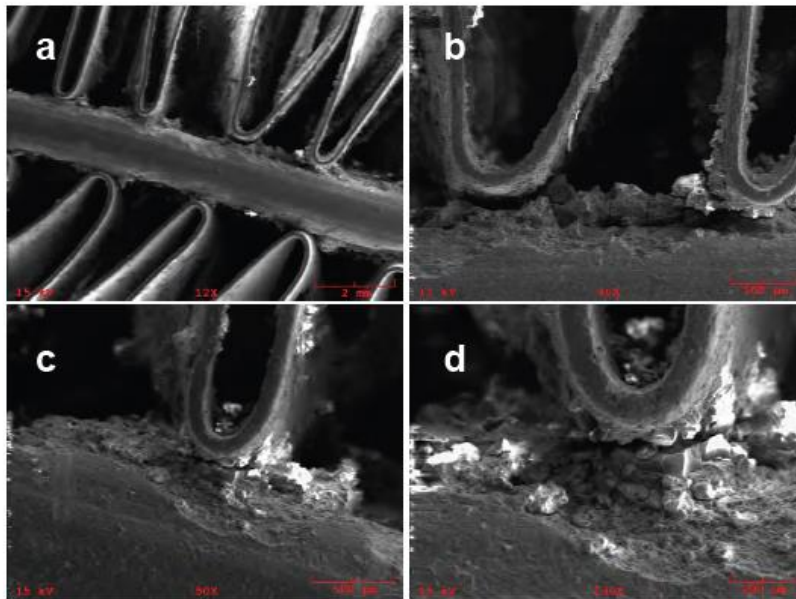


Fig. 9. SEM micrographs of MCHE sample after around 104 days of exposure to corrosive electrolyte [25]

Figure 10 provides insights into the velocity, temperature, and pressure profiles within the fluid domain along the centerline of the circular MCHE for three distinct fin geometries. Figure 10(a) demonstrates the highest velocity observed in the step and saw fin geometries, reaching nearly twice the inlet velocity of the microchannel. Figure 10(b) reveals a temperature decrease of 10-16% in the microchannel fluid for all fin geometries. Despite employing the same microchannel, variations in temperature drop occur throughout the microchannel for different fin geometries. The louver shape fin exhibits the highest temperature drop, suggesting that it excels in transferring heat to the surrounding air and enhancing heat transfer efficiency. Figure 10(c) indicates that all fin geometries result in nearly identical pressure drops. The solid domain, microchannel flow, and crossflow field were tightly coupled to predict the microchannel's temperature, pressure, and velocity distribution. Temperature variation is observed in the microchannel due to the variation of the crossflow around the solid.

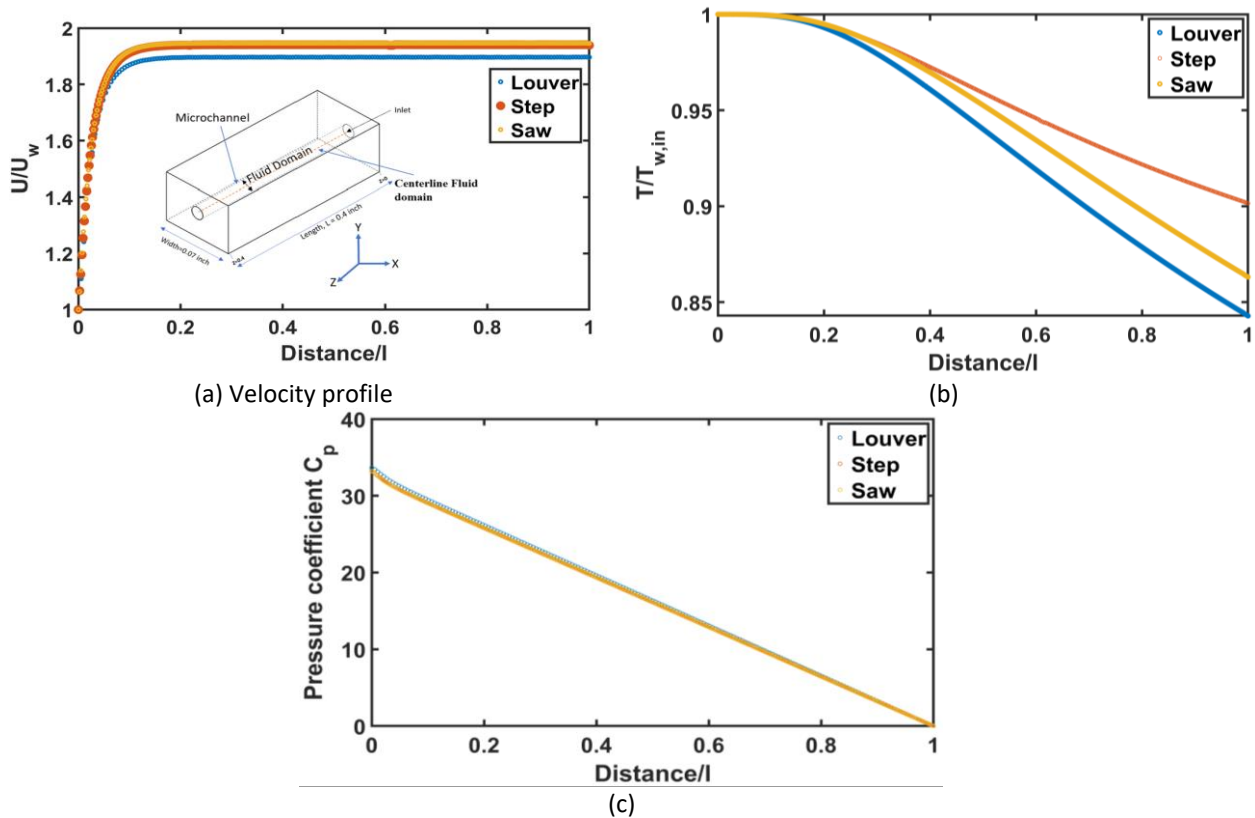


Fig. 10. Fluid domain through the centerline of circular MCHE for different fin geometries (a) Velocity profile (b) Temperature profile (c) Pressure profile

Table 4 displays the thermal performance of tubes featuring fins of louver, step, and saw geometries, with the louver fin demonstrating the highest thermal effectiveness, while the step geometry exhibits the lowest thermal effectiveness.

Table 4
 Effectiveness of MCHE for different fin geometries

Fin Geometry	Effectiveness (ϵ)
Louver	0.337
Step	0.20737
Saw	0.2895

4. Conclusions

This study conducted a numerical investigation to examine the impact of corrosion on fin-and-tube All Aluminum MCHE with various fin geometries. The focus was on analyzing the corrosion hot spots, specifically pitting and crevice corrosion regions, while considering the influence of the external airflow. The results revealed that the louver shape fin emerged as the optimal choice for a circular microchannel, exhibiting fewer corrosion hot spots and superior thermal effectiveness

Acknowledgement

This research was not funded by any grant.

References

- [1] Lachowicz, Marzena M., Maciej B. Lachowicz, and Adam Gertruda. "Role of microstructure in corrosion of microchannel heat exchangers." *Inzynieria Mater. Mater. Eng* 39 (2018): 94-99.
- [2] Guo, Longjun, Jihui Wang, Wenbin Hu, and Dejing Zhou. "Corrosion process of multilayer aluminum-brazed sheet by Eis and En techniques." *Surface Review and Letters* 26, no. 06 (2019): 1850203. <https://doi.org/10.1142/S0218625X18502037>
- [3] Yuan, Zhipeng, Fangyun Tao, Jie Wen, and Yiyu Tu. "The dependence of microstructural evolution and corrosion resistance of a sandwich multi-layers brazing sheets on the homogenization annealing." *IEEE Access* 7 (2019): 121388-121394. <https://doi.org/10.1109/ACCESS.2019.2933740>
- [4] Marshall, G. J., R. K. Bolingbroke, and A. Gray. "Microstructural control in an aluminum core alloy for brazing sheet applications." *Metallurgical Transactions A* 24 (1993): 1935-1942. <https://doi.org/10.1007/BF02666328>
- [5] Yuan, Zhipeng, Yiyu Tu, Han He, Ting Yuan, Quancheng Zhang, and Xiaotong Peng. "Influence of final annealing temperature on the microstructural evolution and corrosion resistance of a Sandwich multi-layered aluminum sheet." *Materials Research Express* 6, no. 2 (2018): 026536. <https://doi.org/10.1088/2053-1591/aee58>
- [6] Kim, Yong-Sang, In-Jun Park, and Jung-Gu Kim. "Simulation Approach for Cathodic Protection Prediction of Aluminum Fin-Tube Heat Exchanger Using Boundary Element Method." *Metals* 9, no. 3 (2019): 376. <https://doi.org/10.3390/met9030376>
- [7] Ali, Murad, Anwar Ul-Hamid, Luai M. Alhems, and Aamer Saeed. "Review of common failures in heat exchangers—Part I: Mechanical and elevated temperature failures." *Engineering Failure Analysis* 109 (2020): 104396. <https://doi.org/10.1016/j.engfailanal.2020.104396>
- [8] Faes, Willem, Steven Lecompte, Zaaquib Yunus Ahmed, Johan Van Bael, Robbe Salenbien, Kim Verbeken, and Michel De Paepe. "Corrosion and corrosion prevention in heat exchangers." *Corrosion reviews* 37, no. 2 (2019): 131-155. <https://doi.org/10.1515/corrrev-2018-0054>
- [9] Yoshino, Michihide, Shohei Iwao, Masakazu Edo, and Hajime Chiba. "Mechanism of intergranular corrosion of brazed Al–Mn–Cu alloys with various Si content." *Materials Transactions* 58, no. 5 (2017): 768-775. <https://doi.org/10.2320/matertrans.L-M2017808>
- [10] Revie, R. Winston. *Corrosion and corrosion control: an introduction to corrosion science and engineering*. John Wiley & Sons, 2008. <https://doi.org/10.1002/9780470277270>
- [11] Mujumdar, Arun S. "Heat Exchanger Design Handbook T. Kuppam Marcel Dekker Inc., New York 2000, 1118 pages." *Drying Technology* 18, no. 9 (2000): 2167-2168. <https://doi.org/10.1080/07373930008917833>
- [12] Roberge, Pierre R. *Handbook of corrosion engineering*. McGraw-Hill Education, 2019.
- [13] Ranjbar, Khalil. "Effect of flow induced corrosion and erosion on failure of a tubular heat exchanger." *Materials & Design* 31, no. 1 (2010): 613-619. <https://doi.org/10.1016/j.matdes.2009.06.025>
- [14] Chen, C. S., and W. J. Kuo. "Heat transfer characteristics of gaseous flow in long mini-and microtubes." *Numerical Heat Transfer, Part A: Applications* 46, no. 5 (2004): 497-514. <https://doi.org/10.1080/10407780490463773>
- [15] Yeo, Ilhwan, and Seunghyun Lee. "2D computational investigation into transport phenomena of subcooled and saturated flow boiling in large length to diameter ratio micro-channel heat sinks." *International Journal of Heat and Mass Transfer* 183 (2022): 122128. <https://doi.org/10.1016/j.ijheatmasstransfer.2021.122128>
- [16] Park, Kyoungwoo, Kwan-Joong Noh, and Kwan-Soo Lee. "Transport phenomena in the thin-film region of a micro-channel." *International Journal of Heat and Mass Transfer* 46, no. 13 (2003): 2381-2388. [https://doi.org/10.1016/S0017-9310\(02\)00541-0](https://doi.org/10.1016/S0017-9310(02)00541-0)
- [17] Sun, Hongwei, and Mohammad Faghri. "Effect of surface roughness on nitrogen flow in a microchannel using the direct simulation Monte Carlo method." *Numerical Heat Transfer: Part A: Applications* 43, no. 1 (2003): 1-8. <https://doi.org/10.1080/10407780307302>
- [18] Beskok, Ali. "Validation of a new velocity-slip model for separated gas microflows." *Numerical Heat Transfer, Part B: Fundamentals* 40, no. 6 (2001): 451-471. <https://doi.org/10.1080/104077901753306593>
- [19] Suman, Balram. "A steady state model and maximum heat transport capacity of an electrohydrodynamically augmented micro-grooved heat pipe." *International journal of heat and mass transfer* 49, no. 21-22 (2006): 3957-3967. <https://doi.org/10.1016/j.ijheatmasstransfer.2006.04.011>
- [20] Fung, Chang Kai, and Mohd Fadhil Majnis. "Computational Fluid Dynamic Simulation Analysis of Effect of Microchannel Geometry on Thermal and Hydraulic Performances of Micro Channel Heat Exchanger." *Journal of Advanced Research in Fluid Mechanics and Thermal Sciences* 62, no. 2 (2019): 198-208.
- [21] Phu, Nguyen Minh, and Pham Ba Thao. "Thermohydraulic performance of a fin and inclined flat tube heat exchanger: A numerical analysis." *CFD Letters* 13, no. 7 (2021): 1-12. <https://doi.org/10.37934/cfdl.13.7.112>

- [22] Hasan, Mushtaq I., Abdul A. Rageb, M. Yaghoubi, and Homayon Homayoni. "Influence of channel geometry on the performance of a counter flow microchannel heat exchanger." *International Journal of Thermal Sciences* 48, no. 8 (2009): 1607-1618. <https://doi.org/10.1016/j.ijthermalsci.2009.01.004>
- [23] Bahiraei, Mehdi, and Ali Monavari. "Thermohydraulic characteristics of a micro plate heat exchanger operated with nanofluid considering different nanoparticle shapes." *Applied Thermal Engineering* 179 (2020): 115621. <https://doi.org/10.1016/j.applthermaleng.2020.115621>
- [24] Bahiraei, Mehdi, Mohammad Naseri, and Ali Monavari. "A CFD study on thermohydraulic characteristics of a nanofluid in a shell-and-tube heat exchanger fitted with new unilateral ladder type helical baffles." *International Communications in Heat and Mass Transfer* 124 (2021): 105248. <https://doi.org/10.1016/j.icheatmasstransfer.2021.105248>
- [25] Nasrazadani, S., H. Vaughan, D. Ellerbrock, and C. Martin-Callizo. "Development of a New Accelerated Corrosion Test for All-Aluminum Microchannel and Tube and Fin Heat Exchangers—Part II: Chamber Study." *ASHRAE Transactions* 126, no. 2 (2020).